Hindawi
Journal of Nanomaterials
Volume 2020, Article ID 7946853, 11 pages
https://doi.org/10.1155/2020/7946853

Research Article

Efficient All-Inorganic $CsPbBr_3$ Perovskite Solar Cells by Using CdS/CdSe/CdS Quantum Dots as Intermediate Layers

Shibing Zou and Feng Li

Engineering Laboratory for Optoelectronics Testing Technology, Nanchang Hangkong University, Nanchang 330063, China

Correspondence should be addressed to Feng Li; lifengnchu@163.com

Received 13 March 2020; Accepted 10 April 2020; Published 6 May 2020

Guest Editor: Jialong Duan

Highly efficient all-inorganic perovskite solar cells require a fast charge transfer from $CsPbBr_3$ to TiO_2 to reduce the recombination from trap states. Herein, we insert a CdS/CdSe/CdS quantum dot (QD) layer between the TiO_2 and $CsPbBr_3$ layers to fabricate all-inorganic perovskite solar cells. By tuning the thicknesses of the CdSe layer of CdS/CdSe/CdS QDs, the conduction band (CB) levels can be adjusted to -3.72~-3.87 eV. After inserting the QD intermediate layer, the energy offset between the CB of TiO_2 and $CsPbBr_3$ is reduced, thus leading to a charge transfer rate boost from 0.040×10^9 to 0.059×10^9 s^{-1}. The power conversion efficiency (PCE) of the solar cell with QD intermediate layer achieves 8.64%, which is 20% higher than its counterpart without QDs.

1. Introduction

Hybrid organic-inorganic lead halide perovskite solar cells (PSCs) are promising candidates for commercialization, owing to their extremely high power conversion efficiency (PCE over 22%) and low fabrication cost. Despite recent rapid progress in developing the novel perovskite materials or optimizing the structure of the hybrid PSCs, the unsatisfactory long-term stability of the PSCs and the high cost of the hole-transporting materials hinder their commercialization [1–3]. All-inorganic PSCs are regarded as one of the most hopeful platforms to tackle this issue [4]. As light absorbers, inorganic perovskites such as $CsPbX_3$ (X=I, Br) have high charge-carrier mobility, which is similar to hybrid perovskites [5–7]. Moreover, inorganic lead halides are capable of against humidity and heat, which guarantee their long stability [4, 8–10]. Besides, the light-induced halide segregation that commonly happens in hybrid perovskites does not occur in such all-inorganic PSCs because ions need to overcome higher energy barrier to migrate compared with hybrid ones. Therefore, growing efforts are devoted to developing all-inorganic PSCs, aiming at resolving the challenging faced by hybrid ones.

Hodes et al. first used $CsPbBr_3$ as the light absorber with a typical device structure of FTO/c-TiO_2/m-TiO_2/$CsPbBr_3$/HTM/Au, achieving a PCE of 5.95% and an open-circuit voltage (V_{oc}) of 1.28 V [11]. These parameters are comparable to those MA-containing hybrid PSCs. Later, Liu and his coworkers fabricated an all-inorganic PSC with architecture of FTO/cTiO_2/m-TiO_2/$CsPbBr_3$/carbon in ambient environment without humidity control, reaching a PCE of 6.7% and good tolerance in humid air and extreme temperatures [5]. Tang's group further boosted the PCEs of $CsPbBr_3$ all-inorganic PSCs from 6.7% to 10.6% by using interfacial or compositional engineering [12–14]. Despite these achievements, the charge-carrier trap states within the $CsPbBr_3$ film and the interface still impede the further improvements of the device performances [13, 15]. Therefore, constructing an appropriate interface and enhancing the charge transfer may work in promoting the charge extraction efficiency and passivating the defects.

Quantum dots (QDs) are nanocrystals of several nanometers in diameter, and they are capable of tuning the optical and electronic properties by adjusting the size or composition [16–18]. Evidence has shown that modifying the energy level of QDs has significant impact on interface charge

transfer [15, 19, 20]. Instead of pursuing proper intermediate buffer layers, we intend to design QDs with proper energy band structures to make better energy level alignment between $CsPbBr_3$ and TiO_2 in PSCs because of the featured energy level tunability of the QDs. Many work shows that reducing the energy offset between the donor and the acceptor can accelerate the charge transfer at the interface [21–25]. Herein, we design core/multishell QDs with the conduction band (CB) ranging in -3.72~-3.87 eV. By inserting the QD layer between the TiO_2 and $CsPbBr_3$, we construct a cascade energy alignment, where photoexcited electrons can be extracted efficiently. Arising from the improved charge transfer rate, the optimized device exhibits a PCE of 8.64%, which is 20% higher than the device without QD intermediate layer.

2. Experimental

2.1. Materials. Cadmium oxide (CdO, 99.99%), sulfur (99.9%, powder), tri-n-octylphosphine (TOP, 90%), oleic acid (OA, 99%), selenium (99%, powder), 1-dodecanethiol (DDT, 98%), 1-octadecene (1-ODE, 90%), titanium isopropoxide (AR, 95%), titanic chloride (AR, 99.0%), lead bromide ($PbBr_2$, AR, 99.0%), caesium bromide (CsBr, AR, 99.9%), N,N-dimethylformamide (DMF, AR, 99.5%), methanol (AR, 99.5%), and isopropanol were purchased from Aladdin. All the materials were used as received without further purification.

2.2. Preparation of Precursors. Cationic precursors (0.1 M cadmium oleate ($Cd(OA)_2$) and 0.5 M cadmium oleate ($Cd(OA)_2$)) were prepared by dissolving CdO (4 mmol or 20 mmol) in a mixed solvent of OA (20 mL) and 1-ODE (20 mL) under N_2 atmosphere at 250°C for 30 min, degassing at 150°C for 30 min, and filling with N_2. Anionic precursors (0.1 M TOP-Se) were prepared by dissolving the selenium power (1 mmol) in 10 mL of TOP under N_2 atmosphere at room temperature.

2.3. Synthesis of CdS Seeds. First, 38.5 mg CdO (0.3 mmol) was loaded in a three-neck flask containing 1 mL of OA and 8 mL of 1-ODE at 150°C under N_2 atmosphere. Then the mixture solution was heated to 270°C, and 0.25 M S-ODE (0.5 mL) was rapidly injected into the reaction flask and stayed for 8 min. The resultant nanocrystals were purified twice by the precipitation (ethanol) and redispersion (toluene) method.

2.4. Synthesis of CdS/CdSe/CdS Nanocrystals. For CdSe emissive layer growth, the desired amount of mixed Cd and Se precursors (0.1 M $Cd(OA)_2$ and 0.1 M TOP-Se) was injected into the three-neck flask containing CdS seeds (0.1 g) and 1-ODE (8 mL) at 300°C at a rate of 10 mL/hr. The obtained CdS/CdSe NCs do not require any purification. For CdS shell growth, the desired amount of 0.5 M $Cd(OA)_2$ and 1 M DDT-ODE were injected separately into the reaction solution at 300°C at a rate of 4 mL/hr. The reaction temperature was maintained at 300°C for the entire CdS shelling process and cooled down to room temperature to stop the reaction. The resultant CdS/CdSe/CdS NCs were purified twice.

2.5. Fabrication of All-Inorganic $CsPbBr_3$ Solar Cells. All-inorganic $CsPbBr_3$ solar cells were prepared according to the previously reported method with some modifications [26]. Typically, 90 μL of CdS/CdSe/CdS solution in toluene was spin-coated onto the FTO/c-TiO_2/m-TiO_2 layer at 2000 rpm for 30 s and heated at 80°C for 10 min. Subsequently, an N,N-dimethylformamide (DMF) solution of 1.0 M $PbBr_2$ was spin-coated onto the CdS/CdSe/CdS layer at 2000 rpm for 30 s, followed by drying at 80°C for 60 min. Then the 0.07 M CsBr methanol solution was spin-coated onto the $PbBr_2$ film at 2000 rpm for 30 s and continuingly heated at 250°C for 5 min. This process was repeated for several times. Finally, the carbon electrode served as both hole transport layer (HTL), and the counter electrode was deposited on the $CsPbBr_3$ layer by doctor-blade coating of conductive carbon ink and then heated at 70°C for 60 min.

3. Results and Discussion

Figure 1(a) illustrates the architecture of the QDs, where a CdS is used as core and a monolayer or multilayer of CdSe grows on the CdS core, followed by growing a thick CdS shell. Both the CB and VB levels of the CdSe are contained between the CB and valence band (VB) of the CdS core and shell. Therefore, the CdS/CdSe/CdS QDs possess a spherical quantum well structure, where the electrons and holes are strongly confined in the CdSe layer. XRD results of the CdS, CdS/CdSe, and CdS/CdSe/CdS QDs are shown in Figure 1(b). The CdS exhibit characteristic peaks at 26.5°, 43.9°, and 51.9°, which are consistent with diffraction angles of the (111, 220, 311) of the standard zinc blende card (JCPDS 01-0647). After coated with CdSe shell, the resultant CdS/CdSe also shows three typical zinc blende diffraction peaks located at 25.61°, 42.89°, and 49.9° with a little shift to those of the CdS core. These XRD results confirm that CdSe shelling does not affect the zinc structure of the CdS just undergoing an epitaxial shell growth of CdSe. However, the growth of the second CdS shell on the zinc blende CdS/CdSe generates a wurtzite crystal structure featured with diffraction peaks at 24.6°, 26.3°, 28.4°, 43.6°, 47.0°, and 52.3°. The presence of the wurtzite structure in this QD is in accordance with some related core/shell systems containing both the wurtzite and zinc blende crystal structures [27]. Transmission electron microscopy (TEM) images from Figures 1(c)–1(f) show that the average diameter increases with the increases of CdSe shell. The TEM images of the prepared QDs display that all QDs have high crystallinity and monodisperse. The average diameters of the QDs are estimated by calculating over 10 TEM images as shown at the bottom of Figure 1. All the QDs are produced from the same CdS core, and the thicknesses of the outer CdS shell are also the same; we denote the QDs as CdS/CdSe(*X* monolayer, *X* ML)/CdS for simplicity. The average diameters of the QDs are determined to be 6.25 nm, 7.25 nm, 8.0 nm, and 11.0 nm for the CdS/CdSe(1 ML)/CdS, CdS/CdSe(3 ML)/CdS, CdS/CdSe(4 ML)/CdS, and CdS/CdSe(6 ML)/CdS, respectively.

Although changing the size of the CdS core or the thickness of CdS can affect the energy structure of the QDs, controlling the thickness of the CdSe offers much wider

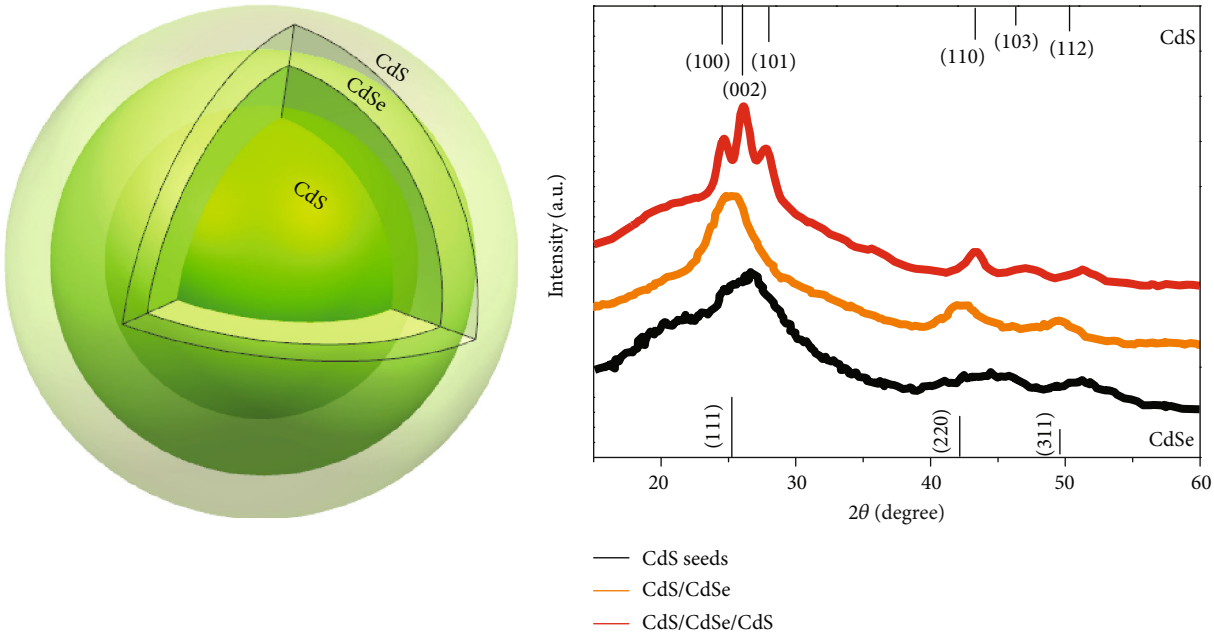

(a) (b)

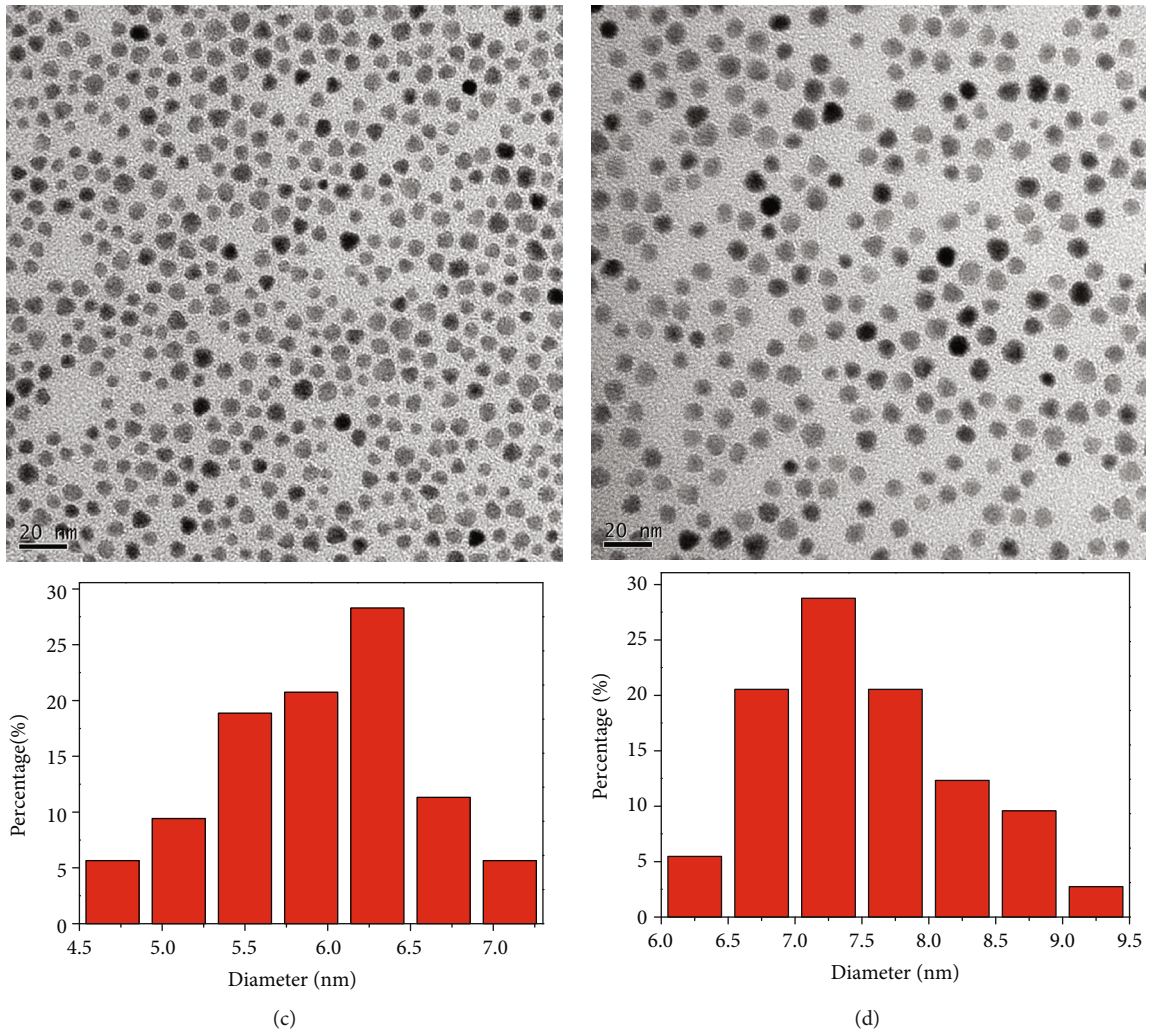

(c) (d)

Figure 1: Continued.

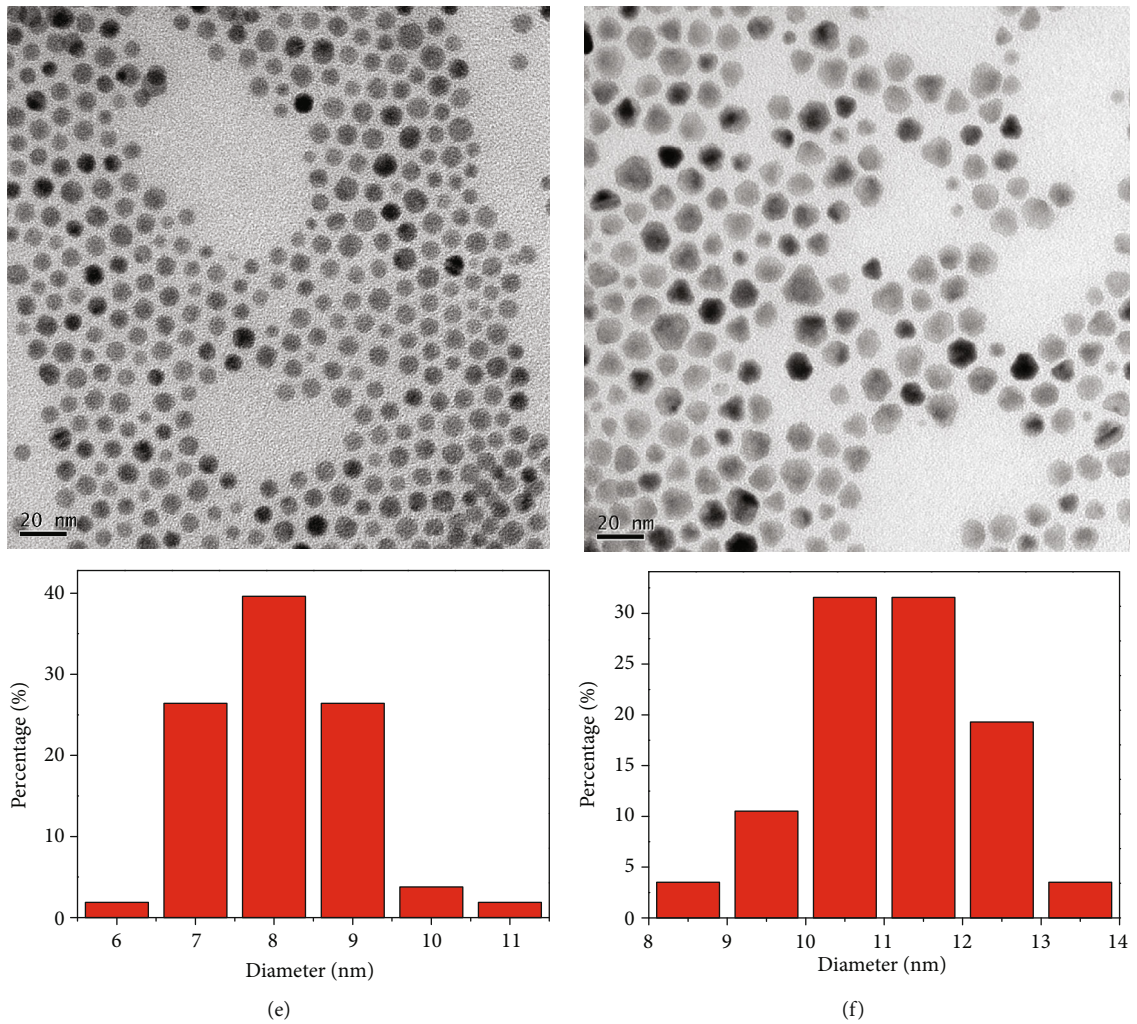

Figure 1: (a) Schematic structures of CdS/CdSe/CdS QD. (b) XRD patterns of CdS seeds, CdS/CdSe, and CdS/CdSe/CdS QDs. (c–f) TEM images of CdS/CdSe/CdS QDs with varying CdSe shell thicknesses (1, 3, 5, and 6 ML) with the corresponding average diameter statistical charts for the QDs.

tenability on the energy levels. CdS has a higher CB and a lower VB than those of CdSe. Therefore, in the CdS/CdSe system, both the hole and electron charges are partially delocalized on the shell materials. Theoretical and experimental results have demonstrated that shell thickness has an influence on the band energy structure of this inverted type I system [28–30]. There is a competition between the kinetic energy and the potential energy in this system. With shell thickness increases, both the electron and the hole wave functions in the center of the particle are increased, while keeping the particle size constant [28]. Hence, the bandgap structure can be adjusted by changing the thickness of CdSe shell. Furthermore, type I and reverse type I QDs usually encounter the predicament of low PL QYs, and type II ones encounter low photooxidation stability. However, QDs with multilayer of shells exhibit both these two high properties [30, 31]. Therefore, a CdS layer was introduced upon the CdS/CdSe QDs to realize the passivation of surface defects. In short, by controlling the thickness of CdSe layer, the CB of CdS/CdSe/CdS QDs can be tuned.

For core/shell QDs, shell usually have a nonnegligible impact on the energy structure, so as to the optical properties of the dots. Many II-IV and I-III-VI core/shell QDs have been synthesized to enhance the stability and the photoluminescence (PL) quantum yields (QYs) of pure cores or to restrain the dot-dot FRET that is beneficial to the improvement of device performance [32–34]. However, there exists a pronounced trade-off between the shell thickness and the PL QYs in the CdSe/CdS system, owing to the traps originated from the exceeded epitaxy of shells. Hence, appropriate shell layers are generally required.

Figures 2(a) and 2(b) show the photoluminescence (PL) spectra of the QDs with different CdSe shell thicknesses. Under the irradiation of an ultraviolet (UV) lamp, the QDs show different color from green to red, indicating the promising tenability of the emission wavelengths. Figure 2(c) shows tunable absorption band edges of the QDs ranging from 580 to 652 nm, corresponding to the bandgaps between 2.14 and 1.90 eV according to the relationship $E_g = 1240/\lambda$ eV. For a conventional inorganic PSC, the energy offset

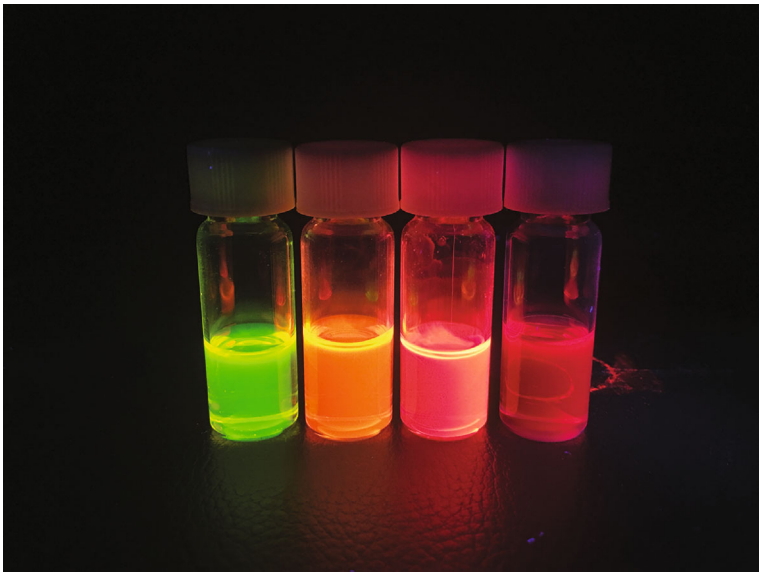

(a)

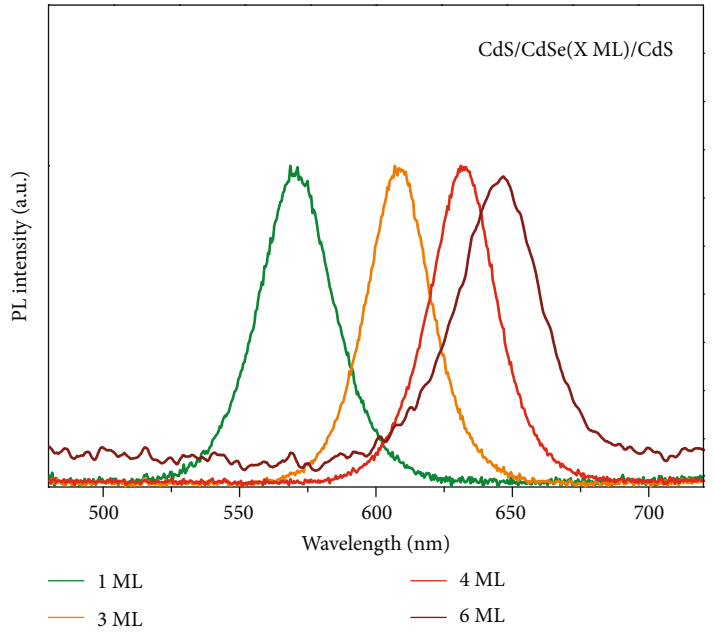

(b)

Figure 2: Continued.

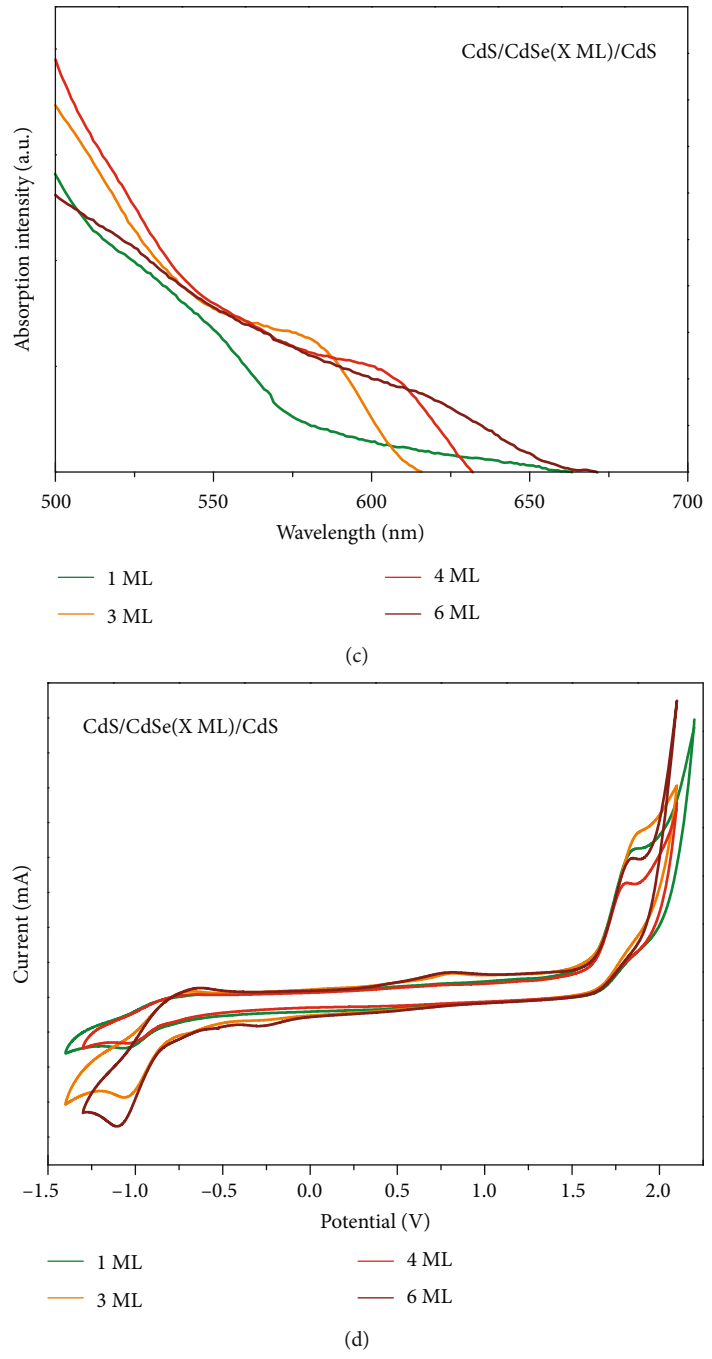

Figure 2: (a) Photograph of CdS/CdSe/CdS solutions under the irradiation of a 365 nm lamp. (b) PL spectra of CdS/CdSe/CdS QDs. (c) Absorption spectra of CdS/CdSe/CdS QDs. (d) CV behaviors of the CdS/CdSe/CdS QDs.

between the CB of $CsPbBr_3$ (-3.30 eV) and TiO_2 (-4.20 eV) is about 0.90 eV, which is large enough to overcome the Coulomb attraction (typically 0.1-0.5 eV) [35]. Gong et al. have demonstrated that electrons can transfer efficiently even with an energy offset as small as 0.12 eV [36]. This prompts us to employ QD as intermediate layer to reduce the "excess" energy offset between TiO_2 and $CsPbBr_3$. Therefore, we performed CV tests to determine the energy level of the prepared QDs with respect to the vacuum level. Figure 2(d) shows obvious oxidation and reduction waves for all QD films,

Table 1: Electrochemical parameters of the CdS/CdSe/CdS QDs.

CdS/CdSe (X ML)/CdS	E_{Re}(V)/CB (eV)	E_{Ox} (V)/VB (eV)	E_g (eV)
1 ML	-0.75/-3.72	1.55/-6.02	2.30
3 ML	-0.70/-3.77	1.55/-6.02	2.25
4 ML	-0.72/-3.75	1.55/-6.02	2.27
6 ML	-0.60/-3.87	1.55/-6.02	2.15

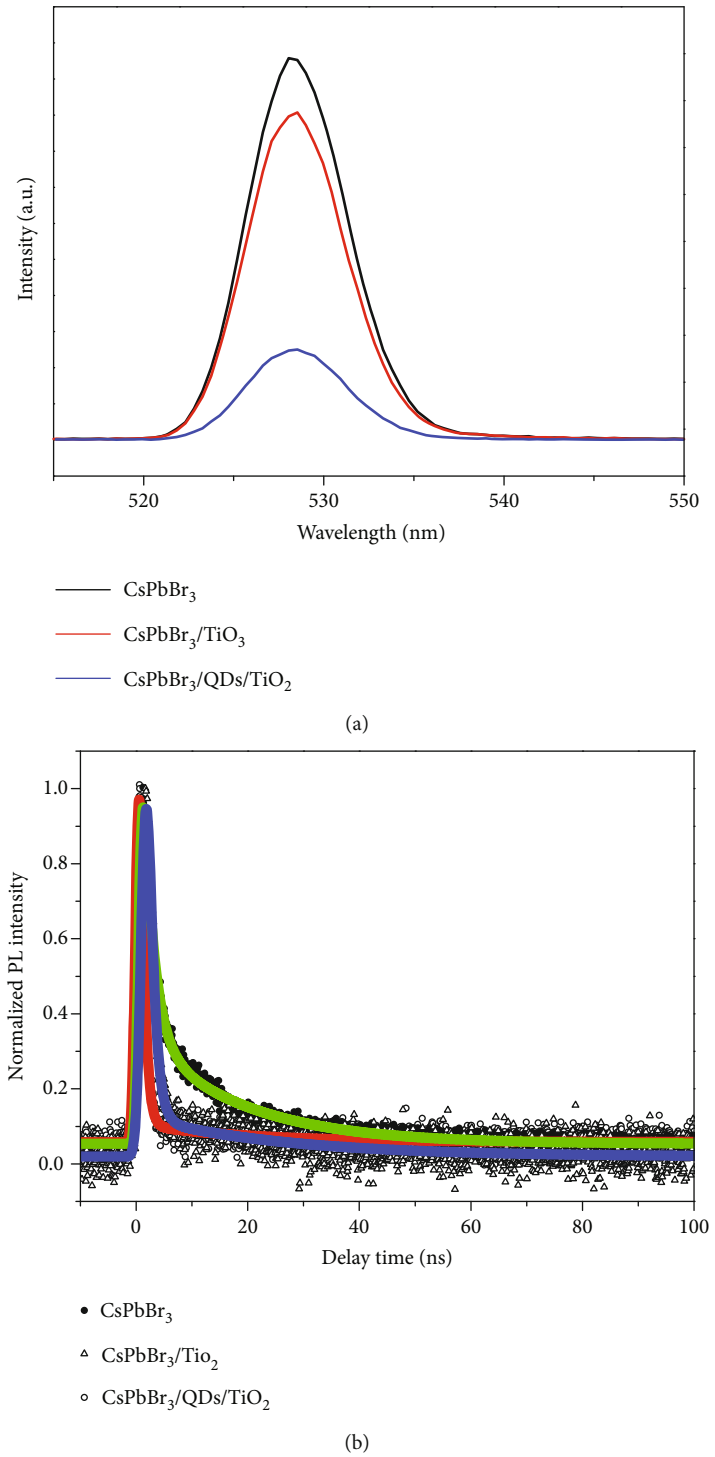

FIGURE 3: (a) Steady PL spectra of $CsPbBr_3$, $CsPbBr_3/TiO_2$, and $CsPbBr_3/QDs/TiO_2$ films. (b) The PL decays of $CsPbBr_3$, $CsPbBr_3/TiO_2$, and $CsPbBr_3/QD/TiO_2$ films.

implying that the QD as an intermediate layer has good capability conducting electrons and holes. The CB and VB levels of the QDs are calculated by using the formula: CB or VB = $-4.8 - (E - E_{1/2})$ (eV), where E is the peak point of the redox potential and $E_{1/2}$ is the formal ferrocene potential against the Ag/Ag^+ system and determined to be $E_{1/2} = 0.33$ eV. The electrochemical parameters of the QDs are summarized in Table 1. With the increase of the thicknesses of the CdSe shell, the CB level changes from -3.72 to -3.87 eV, whereas the VB level varies little as compared with the CB level. Similar results are observed for other QD systems. All the CB levels of the QDs locate between the CB of $CsPbBr_3$

Table 2: Lifetimes and charge transfer rate estimated from PL decays.

Kinetic parameters	a_1	τ_1 (ns)	a_2	τ_2 (ns)	τ (ns)	k_{ct} ($\times 10^9$ s^{-1})
Pristine $CsPbBr_3$	0.81	1.90 ± 0.05	0.20	17.7 ± 0.5	12.4 ± 0.5	
$CsPbBr_3/TiO_2$	0.91	0.9 ± 0.1	0.1	13 ± 1	8.3 ± 1	0.040
$CsPbBr_3/QDs/TiO_2$	0.95	0.6 ± 0.1	0.04	14 ± 1	7.2 ± 1	0.059

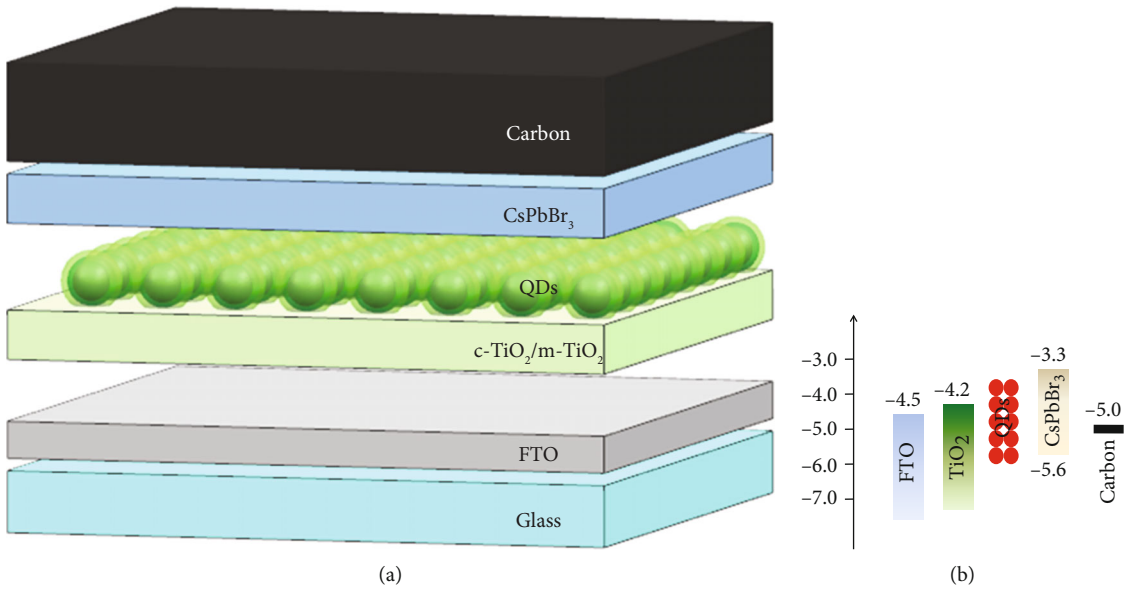

Figure 4: The architecture of all-inorganic $CsPbBr_3$ perovskite solar cell using CdS/CdSe/CdS QDs as an electron modification layer. (b) The schematic diagram of the energy level structure of the PSC.

(-3.3 eV) and the CB of TiO_2 (-4.2 eV). We expect that inserting the QD layer between $CsPbBr_3$ and TiO_2 will reduce the excess energy offset and benefit the electron extraction.

To explore the influences of the QD layer on the charge transfer properties of the solar cell, steady state PL and time-resolved PL measurements were performed. Comparative analysis on $CsPbBr_3/QDs/TiO_2$ against $CsPbBr_3/TiO_2$ enables us identify the role of QDs that plays on the interface charge transfer. Figure 3(a) shows that the PL intensity of the $CsPbBr_3$ decreases notably when interfaced with TiO_2, but inserting the QDs between $CsPbBr_3$ and TiO_2 can further quench the PL intensity. The degree of the PL intensity quenching is quite sensitive to the charge transfer from $CsPbBr_3$ to TiO_2. Such a high degree of PL quenching indicates the strong charge transfer of the $CsPbBr_3/QDs/TiO_2$. To evaluate the exact charge transfer rate at the interface, time-resolved PL measurements were performed, and the results are shown in Figure 3(b). Interfaced with the TiO_2 layer, the emission decays dramatically. An additional intermediate QD layer results in a fastest decay as compared with the neat $CsPbBr_3$ and $CsPbBr_3/TiO_2$ blend. Analyzing the slope of the decay curves, we found that the biexponential function is satisfactory to fit the decays [37]:

$$I(t) = [a_1 \exp(-t/\tau_1) + a_2 \exp(-t/\tau_2)] \otimes F(t), \quad (1)$$

where signal $I(t)$ is the convolution of the biexponential function and the impulse response function (IRF) $F(t)$, a_1 and a_2 are the amplitudes, and τ_1 and τ_2 are lifetimes. Then the average lifetimes are calculated by

$$\tau = \frac{a_1\tau_1^2 + a_2\tau_2^2}{a_1\tau_1 + a_2\tau_2}. \quad (2)$$

Comparing the average lifetime of the $CsPbBr_3$, $CsPbBr_3/TiO_2$, and $CsPbBr_3/QD/TiO_2$ blend films, we can evaluate the interface charge transfer rate k_{ct} by using

$$k_{ct} = \frac{1}{\tau_{blend}} - \frac{1}{\tau_{CsPbBr_3}}. \quad (3)$$

All the kinetic parameters are listed in Table 2. The average decay time t of the neat $CsPbBr_3$, $CsPbBr_3/TiO_2$, and $CsPbBr_3/QDs/TiO_2$ is 12.4, 8.3, and 7.2 ns, respectively. Strikingly, the charge transfer rate of $CsPbBr_3/QDs/TiO_2$ is 0.059×10^9 s^{-1}, which is over 40% faster than that of $CsPbBr_3/TiO_2$.

Figure 4(a) illustrates the device architecture of the all-inorganic PSC with FTO/c-TiO_2/m-TiO_2/QDs/$CsPbBr_3$/carbon configuration. Unlike other PSCs that need hole-transporting layers (HTLs), our all-inorganic PSCs are

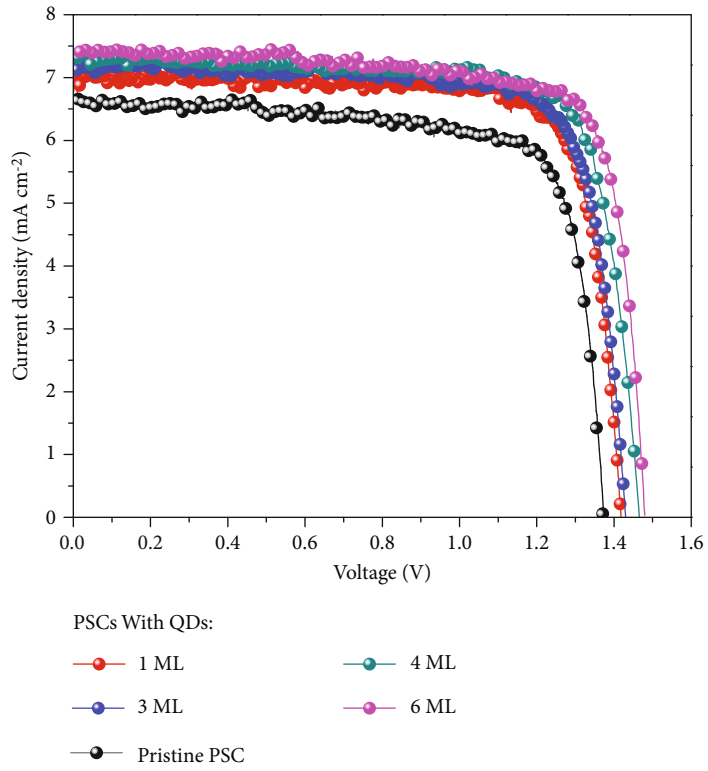

Figure 5: $J - V$ curves of all-inorganic PSCs with and without CdS/CdSe/CdS QDs intermediate layer.

HTL-free. The QDs are used as an intermediate layer between TiO_2 and $CsPbBr_3$. As displayed in Figure 4(b), the CB levels of the QDs range in -3.72~-3.87 eV, which locate above the CB of TiO_2 (-4.2 eV), implying that the QDs are electronically active for electron transfer. Inserting the QD layer also creates a cascade energy level architecture where the energy offset is lowered, which may accelerate the charge transfer process and direct the charge-carriers to circuit. Figure 5 shows the current density-voltage ($J - V$) curves of the all-inorganic PSCs under the illumination of the simulated sunlight (AM1.5G). The photovoltaic parameters of the PSC with different QDs are summarized in Table 3, including open-circuit voltage (V_{oc}), short-circuit current density (J_{sc}), and filling factor (FF). The pristine $CsPbBr_3$ PSC delivers a moderate PCE of 7.15% ($V_{oc} = 1.368$ V, $J_{sc} = 6.69$ mA cm^{-2}, and $FF = 0.78$), which is comparable to other HTL-free inorganic PSCs [8, 15]. After inserting the QDs as intermediate layers, all the devices yield higher J_{sc}, V_{oc}, and PCE than that of the reference device. The underlying mechanism of this enhancement is that the cascade energy level is formed by inserting QDs with appropriate CB level between the CB of TiO_2 and $CsPbBr_3$, thus offering fast charge transfer channel to gain efficient charge extraction. As a consequence, the champion PSC with QDs shows a PCE of 8.64%, which is 20% higher than that of pristine $CsPbBr_3$ PSC.

Table 3: The photovoltaic data of all-inorganic PSCs.

PSCs	J_{sc} (mA cm^{-2})	V_{oc} (V)	FF	PCE (%)
Pristine	6.69	1.368	0.78	7.15
With QDs (1 ML)	7.14	1.419	0.78	7.92
With QDs (3 ML)	7.34	1.431	0.77	8.09
With QDs (4 ML)	7.38	1.466	0.78	8.47
With QDs (6 ML)	7.50	1.482	0.78	8.64

4. Conclusion

In summary, we have synthesized CdS/CdSe/CdS QDs with tunable energy levels and used them as intermediate layers to enhance the performances of the inorganic PSCs. Evidence show that the CB level lies between the CB of TiO_2 and the CB of $CsPbBr_3$, which is suitable for transporting electrons. After inserting the QD intermediate layer, the CB energy offset between TiO_2 and $CsPbBr_3$ is reduced, thus leading to charge transfer rates boosting from 0.040×10^9 to 0.059×10^9 s^{-1}. The optimized PSC shows a PCE as high as 8.64%, which is over 20% higher than 7.15% for the pristine device. This work offers potential route to design HTL-free inorganic PSCs with efficient charge transfer.

Data Availability

Findings of this research work will be provided from corresponding author on reasonable demand.

Conflicts of Interest

The authors declare no conflicts of interest.

Acknowledgments

We gratefully acknowledge the financial support from the Natural Science Foundation of Jiangxi Province (20181BAB202028 and 20192BBF60001).

References

[1] W. S. Yang, B.-W. Park, E. H. Jung et al., "Iodide management in formamidinium-lead-halide-based perovskite layers for efficient solar cells," *Science*, vol. 356, no. 6345, pp. 1376–1379, 2017.

[2] N. J. Jeon, J. H. Noh, W. S. Yang et al., "Compositional engineering of perovskite materials for high-performance solar cells," *Nature*, vol. 517, no. 7535, pp. 476–480, 2015.

[3] Y. Liu, S. Akin, L. Pan et al., "Ultrahydrophobic 3D/2D fluoroarene bilayer-based water-resistant perovskite solar cells with efficiencies exceeding 22%," *Science Advances*, vol. 5, no. 6, p. eaaw2543, 2019.

[4] Y. Wang, M. I. Dar, L. K. Ono et al., "Thermodynamically stabilized β-$CsPbI_3$–based perovskite solar cells with efficiencies >18%," *Science*, vol. 365, no. 6453, pp. 591–595, 2019.

[5] J. Liang, C. Wang, Y. Wang et al., "All-inorganic perovskite solar cells," *Journal of the American Chemical Society*, vol. 138, no. 49, pp. 15829–15832, 2016.

[6] J. Liang, P. Zhao, C. Wang et al., "CsPb0.9Sn0.1IBr2Based all-inorganic perovskite solar cells with exceptional efficiency and stability," *Journal of the American Chemical Society*, vol. 139, no. 40, pp. 14009–14012, 2017.

[7] X. Chang, W. Li, L. Zhu et al., "Carbon-based CsPbBr3Perovskite solar cells: all-ambient processes and high thermal stability," *ACS Applied Materials & Interfaces*, vol. 8, no. 49, pp. 33649–33655, 2016.

[8] X. Zhang, Z. Jin, J. Zhang et al., "All-ambient processed binary CsPbBr3–CsPb2Br5Perovskites with synergistic enhancement for High-Efficiency Cs–Pb–Br-Based solar cells," *ACS Applied Materials & Interfaces*, vol. 10, no. 8, pp. 7145–7154, 2018.

[9] C. Liu, W. Li, C. Zhang, Y. Ma, J. Fan, and Y. Mai, "All-inorganic CsPbI2Br perovskite solar cells with high efficiency exceeding 13%," *Journal of the American Chemical Society*, vol. 140, no. 11, pp. 3825–3828, 2018.

[10] J. Duan, H. Xu, W. E. I. Sha et al., "Inorganic perovskite solar cells: an emerging member of the photovoltaic community," *Journal of Materials Chemistry A*, vol. 7, no. 37, pp. 21036–21068, 2019.

[11] M. Kulbak, S. Gupta, N. Kedem et al., "Cesium enhances long-term stability of lead bromide perovskite-based solar cells," *Journal of Physical Chemistry Letters*, vol. 7, no. 1, pp. 167–172, 2016.

[12] J. Duan, Y. Zhao, B. He, and Q. Tang, "High-purity inorganic perovskite films for solar cells with 9.72 % efficiency," *Angewandte Chemie International Edition*, vol. 57, no. 14, pp. 3787–3791, 2018.

[13] J. Ding, J. Duan, C. Guo, and Q. Tang, "Toward charge extraction in all-inorganic perovskite solar cells by interfacial engineering," *Journal of Materials Chemistry A*, vol. 6, no. 44, pp. 21999–22004, 2018.

[14] J. Duan, Y. Zhao, X. Yang, Y. Wang, B. He, and Q. Tang, "Lanthanide ions doped CsPbBr3Halides for HTM-free 10.14%-efficiency inorganic perovskite solar cell with an ultrahigh open-circuit voltage of 1.594 V," *Advanced Energy Materials*, vol. 8, no. 31, article 1802346, 2018.

[15] G. Liao, J. Duan, Y. Zhao, and Q. Tang, "Toward fast charge extraction in all-inorganic $CsPbBr_3$ perovskite solar cells by setting intermediate energy levels," *Solar Energy*, vol. 171, pp. 279–285, 2018.

[16] X. Jin, H. Li, S. Huang et al., "Bright alloy type-II quantum dots and their application to light-emitting diodes," *Journal of Colloid and Interface Science*, vol. 510, pp. 376–383, 2018.

[17] O. Chen, J. Zhao, V. P. Chauhan et al., "Compact high-quality CdSe-CdS core-shell nanocrystals with narrow emission linewidths and suppressed blinking," *Nature Materials*, vol. 12, no. 5, pp. 445–451, 2013.

[18] C. Pu and X. Peng, "To battle surface traps on CdSe/CdS core/-shell nanocrystals: shell isolation versus surface treatment," *Journal of the American Chemical Society*, vol. 138, no. 26, pp. 8134–8142, 2016.

[19] W. Cao, C. Xiang, Y. Yang et al., "Highly stable QLEDs with improved hole injection via quantum dot structure tailoring," *Nature Communications*, vol. 9, no. 1, p. 2608, 2018.

[20] G. S. Selopal, H. Zhao, X. Tong et al., "Highly stable colloidal "giant" quantum dots sensitized solar cells," *Advanced Functional Materials*, vol. 27, no. 30, article 1701468, 2017.

[21] X. Jin, W. Sun, S. Luo et al., "Energy gradient architectured praseodymium chalcogenide quantum dot solar cells: towards unidirectionally funneling energy transfer," *Journal of Materials Chemistry A*, vol. 3, no. 47, pp. 23876–23887, 2015.

[22] Q. Li, X. Jin, X. Yang et al., "Reducing the excess energy offset in organic/inorganic hybrid solar cells: toward faster electron transfer," *Applied Catalysis B: Environmental*, vol. 162, pp. 524–531, 2015.

[23] X. Jin, W. Sun, Z. Chen et al., "Exciton generation/dissociation/charge-transfer enhancement in inorganic/organic hybrid solar cells by robust single nanocrystalline LnP_xO_y (Ln = Eu, Y) doping," *ACS Applied Materials & Interfaces*, vol. 6, no. 11, pp. 8771–8781, 2014.

[24] F. Li, J. Wei, G. Liao et al., "Quaternary quantum dots with gradient valence band for all-inorganic perovskite solar cells," *Journal of Colloid and Interface Science*, vol. 549, pp. 33–41, 2019.

[25] M. Cha, P. da, J. Wang et al., "Enhancing perovskite solar cell performance by interface engineering using CH3NH3PbBr0.9I2.1Quantum dots," *Journal of the American Chemical Society*, vol. 138, no. 27, pp. 8581–8587, 2016.

[26] B. G. Jeong, Y.-S. Park, J. H. Chang et al., "Colloidal spherical quantum wells with near-unity photoluminescence quantum yield and suppressed blinking," *ACS Nano*, vol. 10, no. 10, pp. 9297–9305, 2016.

[27] B. Mahler, N. Lequeux, and B. Dubertret, "Ligand-controlled polytypism of thick-shell CdSe/CdS nanocrystals," *Journal of the American Chemical Society*, vol. 132, no. 3, pp. 953–959, 2010.

[28] J. W. Haus, H. S. Zhou, I. Honma, and H. Komiyama, "Quantum confinement in semiconductor heterostructure nanometer-size particles," *Physical Review B*, vol. 47, no. 3, pp. 1359–1365, 1993.

[29] Z. Pan, H. Zhang, K. Cheng, Y. Hou, J. Hua, and X. Zhong, "Highly efficient inverted type-I CdS/CdSe core/shell structure QD-sensitized solar cells," *ACS Nano*, vol. 6, no. 5, pp. 3982–3991, 2012.

[30] D. Battaglia, J. J. Li, Y. Wang, and X. Peng, "Colloidal two-dimensional systems: CdSe quantum shells and wells," *Angewandte Chemie*, vol. 42, no. 41, pp. 5035–5039, 2003.

[31] R. G. Chaudhuri and S. Paria, "Core/shell nanoparticles: classes, properties, synthesis mechanisms, characterization, and applications," *Chemical Reviews*, vol. 112, no. 4, pp. 2373–2433, 2012.

[32] I. Coropceanu and M. G. Bawendi, "Core/shell quantum dot based luminescent solar concentrators with reduced reabsorption and enhanced efficiency," *Nano Letters*, vol. 14, no. 7, pp. 4097–4101, 2014.

[33] Y. Niu, C. Pu, R. Lai et al., "One-pot/three-step synthesis of zinc-blende CdSe/CdS core/shell nanocrystals with thick shells," *Nano Research*, vol. 10, no. 4, pp. 1149–1162, 2017.

[34] J.-H. Kim and H. Yang, "High-efficiency Cu-In-S quantum-dot-light-emitting device exceeding 7%," *Chemistry of Materials*, vol. 28, no. 17, pp. 6329–6335, 2016.

[35] T. M. Clarke and J. R. Durrant, "Charge photogeneration in organic solar cells," *Chemical Reviews*, vol. 110, no. 11, pp. 6736–6767, 2010.

[36] X. Gong, M. Tong, F. G. Brunetti et al., "Bulk heterojunction solar cells with large open-circuit voltage: electron transfer with small donor-acceptor energy offset," *Advanced Materials*, vol. 23, no. 20, pp. 2272–2277, 2011.

[37] D. McMorrow, W. T. Lotshaw, and G. A. Kenney-Wallace, "Femtosecond optical Kerr studies on the origin of the nonlinear responses in simple liquids," *IEEE Journal of Quantum Electronics*, vol. 24, no. 2, pp. 443–454, 1988.